25th European Photovoltaic Solar Energy Conference and Exhibition /
5th World Conference on Photovoltaic Energy Conversion, 6-10 September 2010, Valencia, Spain

IMPURITY-TO-EFFICIENCY SIMULATOR: PREDICTIVE SIMULATION OF SOLAR CELL EFFICIENCIES BASED ON MEASURED METAL DISTRIBUTION AND CELL PROCESSING CONDITIONS

Jasmin Hofstetter[1], David P. Fenning[2], Mariana I. Bertoni[2], Jean-François Lelièvre[3]
Tonio Buonassisi[2] and Carlos del Cañizo[1]
[1]Instituto de Energía Solar, Universidad Politécnica de Madrid, Avd. Complutense s/n, 28040 Madrid, Spain
e-mail: jasmin.hofstetter.upm.es. Tel: 914533549 - Fax: 915446341
[2]Massachusetts Institute of Technology, 02138 Cambridge, MA, USA
[3] Centro de Tecnología del Silicio Solar (CENTESIL), Eric Kandel, 1 - Getafe, Spain

ABSTRACT: We present a fast and simple 1D simulation tool to predict solar cell performance as a function of the initial iron content and distribution in the as-grown silicon wafer, the time-temperature profiles applied during the fabrication process, and several parameters related to cell architecture. The applied model consists of three parts that are validated by comparison to experimental results from literature. Assuming a time-temperature profile of a standard solar cell fabrication process, we calculate the redistribution of iron and the evolution of minority carrier lifetime for different as-grown Fe distributions. The solar cell performance as a function of the total iron concentration and the final lifetime distribution is also simulated and compared to experimental results for multicrystalline Si.
Keywords: simulation, crystalline silicon solar cell, gettering.

1 INTRODUCTION

Silicon solar cell performance depends strongly on how well the cell fabrication process is matched to the quality of the wafer source material. Because of the non-linear effects of cell processing on the electronic properties of the material, the final charge carrier lifetime measured on a solar cell cannot be easily deduced from the initial lifetime measured on the as-grown wafer [1].

The time-temperature profiles in a standard solar cell process have been developed for electronic grade Si (EG-Si) but are not well-adapted for solar grade Si (SoG-Si) because of the much higher impurity concentrations in SoG-Si. Tentative specifications of the acceptable impurity levels in SoG-Si given standard cell processing can be found in [2, 3]. In EG-Si, the low total concentration of impurity atoms facilitates the complete dissolution of precipitates and the removal of fast-diffusing species, i.e., Fe, Cr, Ni, and Cu, which is accomplished by means of external gettering during phosphorus emitter diffusion. In contrast, because of the high contamination levels in SoG-Si, high-temperature steps have been predicted to lead to only the partial dissolution of metal precipitates during the short phosphorous diffusion gettering (PDG) applied in a typical industrial solar cell process [4, 5]. To extract the full efficiency potential from low-quality wafers, the industrial process needs to be adapted to accommodate SoG-Si, as well as to enhance performance of cells originating from areas of the ingot that contain higher impurity contents (e.g., edge, top and bottom regions). In these "red zone" areas, iron is usually the dominant impurity [6, 7]. Thus far, the flexible adaptation of the solar cell fabrication process to each source material has been a resource-intensive task due to the lack of predictive capability.

In this manuscript, we present a simulation tool that predicts final solar cell performance given inputs of material quality, cell processing conditions, and cell architecture, as shown in Fig. 1. This "Impurity-to-Efficiency" (I2E) simulator assumes that iron is the dominant lifetime-limiting impurity, an approximation that is accurate in many regions of a standard mc-Si ingot.

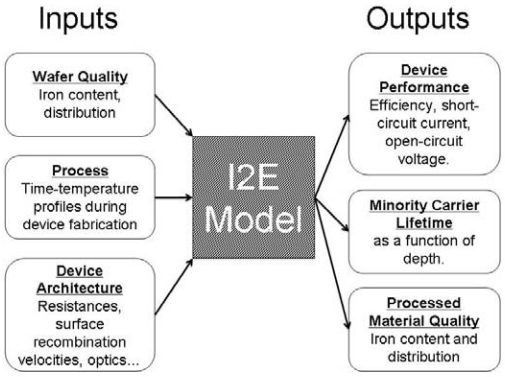

Figure 1: Required inputs and resulting outputs of the I2E simulator

Besides its predictive capability, the integrated I2E model allows one to design a solar cell process adapted to measurable material properties, i. e. total iron concentration and distribution. As an example, the optimization of short extended gettering of highly Fe-contaminated mc-Si border wafers is discussed in [8]. The model can serve as a guide to researchers and manufacturers working toward optimizing processing parameters, saving time and money.

2 MODEL DESCRIPTION

Our I2E simulator, as shown in Fig. 1, calculates the impact of impurity content and distribution on final cell efficiency as a function of thermal processing. It consists of three standalone modeling blocks: (A) a diffusion-gettering simulator that models the evolution of iron distribution during cell processing, (B) a Shockley-Read-Hall-based lifetime model

for converting as-processed Fe_i impurity distribution to effective minority carrier lifetime, and (C) the *PC1D* open-source device simulation software [9].

Our model describes the evolution of the dissolved and precipitated iron distribution during the solar cell fabrication process. It takes into account segregation of iron to a diffused phosphorus layer and the dissolution of iron from iron silicide precipitates. The dissolved iron concentration, $C_i(x,t)$, the phosphorus profile, $P(x,t)$, and the precipitate radius, $r(x,t)$ are modeled along the wafer thickness, x, as a function of processing time, t, using a finite element mesh.

The formation of the typical kink and tail-profile of the P emitter is described by a semi-empirical model developed by Bentzen *et al.* [10]. To describe the kinetics of iron atoms within the silicon, we used the diffusion segregation equation, which was introduced by Tan *et al.* [11]. The space-dependent segregation coefficient of iron in the phosphorus layer has been modeled by applying a semi-empirical model developed by Haarahiltunen *et al.* [12]. To account for the dissolution of precipitated iron atoms, we apply Ham's law [13].

Generally, the total content of a certain metal impurity within the material can be easily determined by bulk analysis, but its distribution, i. e., the mean precipitate density and radius, are unknown parameters and can strongly vary for different Si materials [14]. In this work, we use the as-grown precipitate radius as fit parameter. We assume that the initially precipitated iron $C_{p,0}$ is distributed with a precipitate density, N, and with a mean radius of r_0. To reduce the number of fit parameters over the ingot height in section 3.1, r_0 is assumed to remain constant over the ingot height. In reality, it can vary over the ingot height and also throughout the Si wafer, mainly depending on the density of heterogeneous nucleation sites.

Our model does not take into account the formation of new iron precipitates, i.e., precipitate nucleation. However, the dissolved interstitial iron, Fe_i, is the most detrimental chemical state of iron in Si. As the kinetic model can accurately estimate the flow of Fe_i from precipitates into the bulk, and from the bulk into the highly P-doped surface region, in a first approximation the formation of new precipitates can be ignored for cell processing. However, nucleation cannot be ignored during crystal growth, and any model of impurity distribution during growth must account for nucleation kinetics.

Once the final iron distribution resulting from thermal processing has been calculated, it is translated into a distribution of electron and hole lifetime throughout the wafer thickness. Charge carrier recombination at interstitial iron atoms or at iron-boron (Fe-B) pairs is described by Shockley-Read-Hall statistics under low injection conditions [15, 16]. Recombination at iron silicide precipitates is described by the following expression deduced by Cañizo *et al.* [17]. The complete set of equations used in the model can be found in [18, 19].

Within *PC1D*, the device can be divided into regions of different lifetimes corresponding to the lifetime distribution after solar cell processing. For example, the lifetime regions can be made correspond to the near-surface highly-doped phosphorus layer, the depletion region, and the bulk. The P profile resulting from the diffusion-gettering simulation is imported as an external emitter profile in *PC1D*.

3 MODEL VALIDATION

In the framework of the European Integrated Project *Crystal Clear*, mc-Si ingots were grown from very pure Si that was intentionally contaminated with 53 ppmw of iron [20]. The total and the dissolved iron concentrations, [Fe] and [Fe_i], were measured at different heights along the p-type ingot on as-grown wafers ([Fe_i] corresponds to the mean value over the wafer thickness). Additionally, [Fe_i] was measured on P-diffused samples [21].

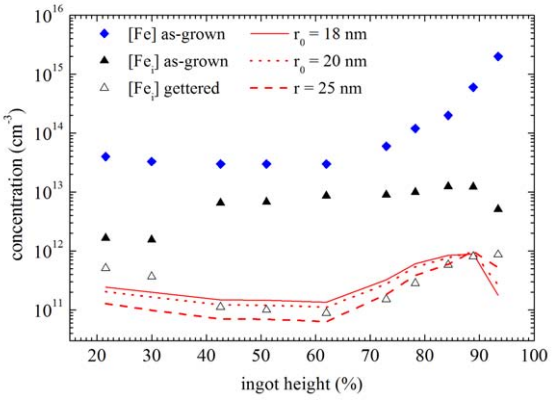

Figure 2: Total and dissolved iron concentrations over the ingot height measured on as-grown wafers (full diamonds and triangles) and [Fe_i] on P-diffused wafers (open triangles) [20, 21] (total [Fe] are interpolated experimental values); calculated [Fe_i] for three different as-grown conditions: a constant as-grown precipitate radius of r_0 = 18 nm, 20 nm and 25 nm.

3.1 Iron diffusion and gettering

We calculated the post-diffusion [Fe_i] along the ingot height (IH), taking the measured [Fe] and [Fe_i] as input parameters for the I2E simulator. As initial condition of the simulation, we specify a constant as-grown radius for all heights such that r_0 = constant and $N = N(IH)$. The measured and calculated values are shown in Fig. 2. As time-temperature profile, a 15 min P diffusion at 850°C followed by an exponential cool down with a cooling rate of 7 min was assumed. The rapid thermal annealing step applied for contact firing has not been simulated as the experimental results show that it has a relatively low impact on the iron distribution [21]. Based on typical values of mean radius in mc-Si [14], three different iron distributions were considered. Constant as-grown precipitate radii of r_0 = 18 nm, 20 nm and 25 nm were chosen, leading to variations of the precipitate density from about $N = 10^7$ to $3{\cdot}10^9$ cm^{-3} over the ingot height.

The trend of the experimental data is very well reflected by all three simulated curves. The larger the initial precipitate radius is chosen, the lower are the final [Fe_i] values. The experimental data points largely fall between the calculated curves for r_0 = 18 nm and r_0 = 25 nm so that they seem to be close to the actual precipitate sizes.

At the bottom of the ingot, the calculated [Fe_i] after PDG is lower than the measured values. In general, the density of both structural defects and oxygen precipitates has been observed to increase towards the ingot bottom, providing many favorable nucleation sites for metal precipitates. In this case, the mc-Si ingot in consideration is a laboratory-scale ingot of only 110 mm height, such that the defective bottom region extends much further into the center of the ingot than for com-

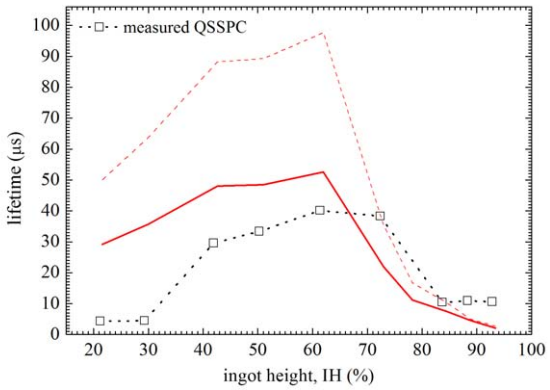

Figure 3: Electron lifetimes measured on P-diffused wafers (open squares) as a function of the ingot height in intentionally Fe-contaminated cast mc-Si; simulated electron lifetimes for as grown radii of $r_0 = 18$ nm (solid line) and $r_0 = 25$ nm (dashed line)

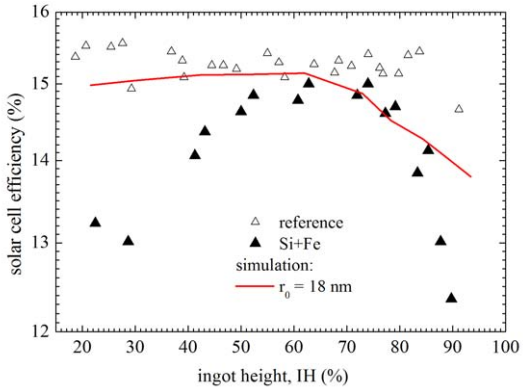

Figure 4: Solar cell efficiency as a function of the ingot height measured on intentionally-contaminated mc-Si (full triangles) and in the reference ingot (open triangales); simulated solar cell efficiency for an as-grown radius of $r_0 = 18$ nm

mercially available mc-Si ingots.

The higher concentration of defects other than Fe in this deteriorated bottom region might be responsible for the poor gettering response observed there. Using our simulation tool to study this potential degradation effect, we find that for a given total [Fe], a higher density of smaller precipitates leads to faster dissolution during high-temperature steps, increasing [Fe_i] locally. Given experimental evidence that areas of high dislocation density respond poorly to PDG with low minority carrier lifetimes remaining after processing [22, 23], we suspect that the locally elevated interstitial iron population at the bottom of the ingot is trapped in the bulk by defect interactions.

The effect of defects other than Fe has not been taken into account in the I2E simulation, where a homogeneous distribution of β-$FeSi_2$ precipitates in each wafer was assumed. The actual distribution of iron precipitates along the height of the ingot has been studied by means of micro- X-Ray Fluorescence and will be discussed and compared to the simulation results in a separate publication [24].

3.2 Charge carrier lifetime

For further model validation, the electron lifetime in P-diffused samples was calculated along the height of the intentionally Fe-contaminated mc-Si ingot of section 3.1 for two as-grown radii, $r_0 = 18$ nm and $r_0 = 25$ nm. The electron lifetime is determined by recombination at dissolved and precipitated iron. It was assumed that all dissolved iron is present in form of Fe-B pairs (lifetime measurement conditions). The corresponding electron capture cross section was taken from [25]. No other lifetime-limiting defects apart from Fe-B pairs and β-$FeSi_2$ precipitates were taken into account. In Fig. 3, the calculated lifetime distributions for as-grown and gettered wafers are plotted as a function of ingot height. The actual effective lifetime values measured by means of Quasi-Steady State Photoconductance on P-diffused samples as reported in [21] are also shown. The measured values are given for an injection level of $\Delta n = 10^{15}$ cm^{-3} while the simulations were done under the assumption of low injection conditions. A potential discrepancy is assumed to be negligible given that the Fe-B pair dominated electron lifetime measured on mc-Si wafers is usually nearly independent of the injection level in this range [26].

The measured lifetime at the bottom of the ingot is much lower than the calculated values. This is attributed to a higher density of oxygen precipitates and crystal defects, which e. g. Coletti *et al.* [21] suggested dominate the minority carrier lifetimes at the bottom of the ingot and are not affected by external gettering.

At the center of the ingot the calculated lifetime values are much closer to the measured ones when a precipitate radius of 18 nm is assumed. As a smaller precipitate radius corresponds to a higher density of precipitates, the electron lifetime is lower due to a higher density of recombination centers. At the top of the ingot, the assumption of larger precipitates with 25 nm radius leads to a better match of the simulated values to the experimental results.

The concentration of dissolved iron after PDG is drastically reduced for both initial as-grown Fe distributions. Therefore, the charge carrier lifetime at the center and top of the ingot also depends on the distribution of precipitated iron. In this case, the knowledge of the as-grown iron distribution is important as it defines the final electron lifetime after gettering and, consequently, solar cell performance.

3.3 From impurity distribution to solar cell efficiency

To validate the I2E model as a whole, the solar cell efficiency along the height of the intentionally contaminated p-type mc-Si ingot was simulated with *PC1D* for a constant as-grown radius of $r_0 = 18$ nm along the ingot heigth. As input parameters, we used the P emitter profile calculated in section 3.1 and further cell parameters published in [21] and [27]. The final charge carrier lifetimes were re-calculated using the minority carrier capture cross sections of interstitial iron, assuming that at one sun illumination all Fe-B pairs are dissociated (solar cell operation conditions).

The simulated efficiency values are compared to measured efficiencies published in [28] and are shown in Fig. 4. As expected from the poor fit of the [Fe_i] and lifetime distribution at the bottom of the ingot (see Figs. 2 and 3), the calculated solar cell efficiencies deviate significantly from the measured

values below 50% ingot height. As mentioned before, this low device performance in the bottom region is most likely due to defects other than iron.

Further comparison of Figs. 3 and 4 show that the decrease in modeled lifetime towards the top of the ingot results in a degradation of the simulated solar cell efficiency. However, for ingot heights $> 80\%$, the measured efficiency degradation is more pronounced and cannot be explained by the decreasing bulk lifetime alone. The additional efficiency degradation is probably due to the drop in the fill factor that has been measured from about 80% ingot height upwards [21]. This drop in the fill factor at the top of the ingot may be due to shunts that arise from either silicon-carbide and silicon-nitride microdefects, metal precipitates, or both. The carbon concentration increases towards the top of the ingot, and SiC microdefects have been shown to lead to important shunt losses [29]. Iron precipitates have been recently observed at voltage prebreakdown sites in mc-Si solar cells as well [30]. Additionally, dendritic crystal growth has been observed for very high iron concentrations towards the ingot top [20], which might favor the formation of such second-phase particles.

Between 50 and 80% ingot height, the simulated efficiency curve matches the experimental data fairly well. Coletti *et al.* showed that in this region the electron diffusion length is dominated by recombination at Fe-related defects [21]. This leads to the conclusion that the I2E model is valid when recombination at Fe-related defects limits the solar cell performance. In that case, the final cell efficiency can be accurately simulated for a known as-grown Fe content and distribution in the wafer.

4 CONCLUSIONS

The Impurity-to-Efficiency (I2E) simulator we have developed allows one to calculate final solar cell performance as a function of the as-grown iron content and distribution in the Si wafer, the time-temperature profiles during solar cell processing, and the device architecture. We have successfully validated the three standalone parts of our model, comparing our simulations to experimental results published on mc-Si materials. The I2E model results provide insight into the different mechanisms that dominate the effectiveness of PDG and the final solar cell performance in highly Fe-contaminated material. Poor device performance associated with wafers from the top of the ingot appears to be strongly influenced by decreases in fill factor, possibly related to shunting, besides the decreased minority carrier lifetime. For novel processing concepts, the I2E simulator can guide towards optimization of time-temperature profiles when a trade-off between efficiency increase and short process time has to be found for highly Fe-contaminated materials.

5 ACKNOWLEDGMENT

This work has been partially funded by the Spanish Ministerio de Ciencia e Innovación through Thincells project (TEC2008-06798-C03-02), by the U.S. Department of Energy, under contract number DE-FG36-09GO19001, and through the generous support of Doug Spreng and the Chesonis Family Foundation. D. P. Fenning acknowledges the support of the NSF Graduate Research Fellowship. The additional support through the MIT-Spain/La Cambra de Barcelona Seed Fund is gratefully acknowledged.

References

[1] L. Carnel, J. Nyhus, K. Helland, PV International 7.

[2] G. Coletti, P. Bronsveld, C. Knopf, C. Swanson, R. Kvande, L. Arnberg, H. Habenicht, W. Warta, in: Proc. 24th EUPVSEC, Hamburg, Germany, 2009.

[3] J. Hofstetter, J. F. Lelièvre, C. del Cañizo, A. Luque, Materials Science and Engineering: B 159-160 (2009) 299–304.

[4] P. Plekhanov, R. Gafiteanu, U. Gösele, J. T.Y. Tan, J. Appl. Phys. 86 (1999) 2453–2458.

[5] A. Haarahiltunen, H. Savin, M. Yli-Koski, H. Talvitie, M. Asghar, J. Sinkkonen, Materials Science and Engineering B.

[6] B. L. Sopori, L. Jastrzebski, T. Tan, in: 25th IEEE PV Specialists Conference, 1996, p. 625.

[7] T. U. Naerland, L. Arnberg, A. Holt, Prog. Photovoltaics res. appl. 17 (2008) 289 – 296.

[8] J. Hofstetter, J. F. Lelièvre, D. P. Fenning, M. I. Bertoni, T. Buonassisi, C. Cañizo, phys. stat. sol. (c) accepted for publication.

[9] P. Basore, D. A. Clungston, Proceedings of the 25th IEEE Photovoltaic Specialists Conference (1996) 377.

[10] A. Bentzen, A. Holt, J. S. Christensen, B. G. Svensson, Journal of applied physics 99 (2006) 064502.

[11] T. Y. Tan, R. Gafiteanu, S. M. Joshi, U. Gösele, Semiconductor Silicon, 1998, p. 1050.

[12] A. Haarahiltunen, H. Savin, M. Yli-Koski, H. Talvitie, J. Sinkkonen, Journal of applied physics 105 (2009) 023510.

[13] F. Ham, J. Phys. Chem. Solids 6 (1958) 335.

[14] T. Buonassisi, A. Istratov, M. Marcus, B. Lai, Z. Cai, S. Heald, E. Weber, Nat. Mater. 4 (2005) 676–679.

[15] W. Shockley, J. W. T. Read, Phys. Rev. 87 (1952) 835–842.

[16] R. N. Hall, Phys. Rev. 87 (1952) 387.

[17] C. del Cañizo, A. Luque, J. Electrochem. Soc. 147 (2000) 2685–2692.

[18] J. Hofstetter, D. P. Fenning, J. F. Lelièvre, M. I. Bertoni, T. Buonassisi, C. del Cañizo, in: 24th EUPVSEC, Hamburg, Germany, 2009.

[19] J. Hofstetter, D. P. Fenning, M. I. Bertoni, J. F. Lelièvre, C. del Cañizo, T. Buonassisi, Prog. Photovoltaics Res. Appl. accepted for publication.

[20] R. Kvande, B. Geerligs, G. Coletti, L. Arnberg, M. D. Sabatino, E. J. Ovrelid, C. C. Swanson, Journal of applied physics 104 (2008) 064905.

[21] G. Coletti, R. Kvande, V. D. Mihailetchi, L. J. Geerligs, L. Arnberg, E. J. Øvrelid, Journal of applied physics 104 (2008) 104913.

[22] M. Kittler, W. Seifert, Solid State Phenomena 95/96 (2004) 197–204.

[23] A. Bentzen, A. Holt, R. Kopecek, G. Stokkan, J. S. Christensen, B. G. Svensson, J. Appl. Phys. 99 (2006) 093509.

[24] D. P. Fenning, J. Hofstetter, M. I. Bertoni, J. F. Lelièvre, G. Coletti, C. del Cañizo, T. Buonassisi, to be sumitted September 2010.

[25] D. Macdonald, T. Roth, P. N. K. Deenapanray, T. Trupke, R. A. Bardos, Applied Physics Letters 89 (2006) 142107.

[26] D. H. Macdonald, L. J. Geerligs, A. Azzizi, J. Appl. Phys. 95 (3) (2004) 1021–1028.

[27] C. Tool, M. Koppes, M. Fleuster, B. van Straaten, A. Weeber, in: Proc. of the 21st EUPVSEC, Dresden, Germany, 2006, p. 1272.

[28] G. Coletti, P. Bronsveld, R. Kvande, L. Geerligs, L. Arnberg, H. Habenicht, W. Warta, C. Knopf, in: 18th Photovoltaic Solar Energy Conference, Kolkata, India, 2009.

[29] J. Bauer, O. Breitenstein, , J.-P. Rakotoniaina, phys. stat. sol. (a) 204 (2007) 2190.

[30] W. Kwapil, P. Gundel, M. C. Schubert, F. D. Heinz, W. Warta, E. R. Weber, A. Goetzberger, G. Martinez-Criado, Applied Physics Letters 95 (2009) 232113.